Clinical Cancer Research

MEIS1 and MEIS2 Expression and Prostate Cancer Progression: A Role For HOXB13 Binding Partners in Metastatic Disease

Raj R. Bhanvadia[1], Calvin VanOpstall[2], Hannah Brechka[2], Nimrod S. Barashi[3], Marc Gillard[3], Erin M. McAuley[4], Juan Manuel Vasquez[5], Gladell Paner[6], Wen-Ching Chan[7], Jorge Andrade[7,8], Angelo M. De Marzo[9], Misop Han[9], Russell Z. Szmulewitz[10], and Donald J. Vander Griend[2,3]

Abstract

Purpose: Germline mutations within the MEIS-interaction domain of HOXB13 have implicated a critical function for MEIS–HOX interactions in prostate cancer etiology and progression. The functional and predictive role of changes in MEIS expression within prostate tumor progression, however, remain largely unexplored.

Experimental Design: Here we utilize RNA expression datasets, annotated tissue microarrays, and cell-based functional assays to investigate the role of MEIS1 and MEIS2 in prostate cancer and metastatic progression.

Results: These analyses demonstrate a stepwise decrease in the expression of both MEIS1 and MEIS2 from benign epithelia, to primary tumor, to metastatic tissues. Positive expression of MEIS proteins in primary tumors, however, is associated with a lower hazard of clinical metastasis (HR = 0.28) after multivariable analysis. Pathway and gene set enrichment analyses identified MEIS-associated networks involved in cMYC signaling, cellular proliferation, motility, and local tumor environment. Depletion of MEIS1 and MEIS2 resulted in increased tumor growth over time *in vivo*, and decreased MEIS expression in both patient-derived tumors and MEIS-depleted cell lines was associated with increased expression of the protumorigenic genes cMYC and CD142, and decreased expression of AXIN2, FN1, ROCK1, SERPINE2, SNAI2, and TGFβ2.

Conclusions: These data implicate a functional role for MEIS proteins in regulating cancer progression, and support a hypothesis whereby tumor expression of MEIS1 and MEIS2 expression confers a more indolent prostate cancer phenotype, with a decreased propensity for metastatic progression. *Clin Cancer Res; 24(15); 3668–80.* ©2018 AACR.

Introduction

Prostate cancer remains a significant cause of morbidity and mortality, and remains the second leading cause of cancer-related death among American men (1). While localized prostate cancer is treated with either surgery or radiation with curative intent, 20%–40% of patients will develop recurrent disease within 10 years (2). Importantly, not all patients with biochemical recurrence have the same prognosis. Physicians face a difficult set of management decisions in balancing prevention of metastatic disease with appropriate therapy and avoidance of overtreatment in patients who may be at low risk for progression to metastatic disease (2). While currently established predictors of prostate cancer recurrence rely on commonly used pathologic criteria, including Gleason grade, there remains a need to identify improved molecular markers of metastatic progression in prostate cancer. Furthermore, there is a critical need for a more thorough understanding of the biologic processes that alter prostate cancer behavior to more successfully risk-stratify and effectively treat patients (3).

MEIS1 and MEIS2 (Myeloid Ecotropic viral Insertion Site) are transcription factors that regulate important functions in cell fate determination during development and cell proliferation. A major function of MEIS proteins is to bind and direct HOX protein transcriptional specificity (4, 5). Importantly, many identified germline *HOXB13* mutations, which confer increased incidence of prostate cancer, occur within the MEIS-interaction domains of HOXB13 (4, 6). Abnormalities in MEIS protein expression and function are implicated in a variety of cancers (4). However, both tumor-suppressive and oncogenic functions of MEIS1 and MEIS2 are reported, but their tumor-regulatory function clearly depends

[1]The Pritzker School of Medicine, The University of Chicago, Chicago, Illinois. [2]The Committee on Cancer Biology, The University of Chicago, Chicago, Illinois. [3]Department of Surgery, Section of Urology, The University of Chicago, Chicago, Illinois. [4]The Committee on Molecular Pathology and Molecular Medicine, The University of Chicago, Chicago, Illinois. [5]The Post-Baccalaureate Research Education Program (PREP), The University of Chicago, Chicago, Illinois. [6]The Department of Pathology, The University of Chicago, Chicago, Illinois. [7]The Center for Research Informatics, The University of Chicago, Chicago, Illinois. [8]The Department of Pediatrics, The University of Chicago, Chicago, Illinois. [9]The Brady Urological Institute, The Johns Hopkins School of Medicine, Baltimore, Maryland. [10]Department of Medicine, Section of Hematology and Oncology, The University of Chicago, Chicago, Illinois.

Note: Supplementary data for this article are available at Clinical Cancer Research Online (http://clincancerres.aacrjournals.org/).

R.R. Bhanvadia and C. VanOpstall contributed equally to this article.

Corresponding Author: Donald J. Vander Griend, The University of Chicago Department of Surgery, The Section of Urology, 5841 S. Maryland Ave, MC6038, Chicago, IL 60637. E-mail: prostate@uchicago.edu

doi: 10.1158/1078-0432.CCR-17-3673

Translational Relevance

Here, we demonstrate that expression of MEIS1 and MEIS2 have a significant role in blocking prostate cancer progression and metastasis. MEIS1 and MEIS2 expression are correlated in clinical data sets, demonstrating that expression of both genes is suppressed during prostate cancer progression. Pathways associated with MEIS expression in the primary tumor include targets of cMYC, proliferation, differentiation, and cell adhesion. In addition, loss of MEIS expression in prostate cancer cells increases tumor growth *in vivo*. These data suggest that MEIS proteins may represent a largely unexplored target for the identification of efficacious targets and the development of future cancer therapeutics.

upon the organ site under investigation (4). For example, increasing MEIS1 expression in non–small cell lung cancer cells results in limited cancer cell proliferation, thus implying a tumor suppressor function. In ovarian cancer, however, MEIS2 expression is negatively associated with patient survival in ovarian cancer, implying an oncogenic function (7, 8). There is limited data on the function of MEIS in the normal and diseased prostate, and given the tissue-specific functions of MEIS, an investigation of MEIS proteins in the prostate has the high potential to significantly enhance our understanding of the etiology of prostate cancer progression. Such studies would represent a critical step in improving therapy decisions for patients, especially after treatment of localized cancer.

We originally identified a role for MEIS proteins in prostate cancer via a screen to identify cancer-associated differences between human prostate and seminal vesicle epithelial cells (9). This was based upon the rationale that there existed critical genes involved in prostate development and tissue homeostasis that strongly predisposed the prostate to carcinogenesis, yet also led to a significant lack of cancer initiation in the seminal vesicle (10, 11). This approach identified both MEIS1 and MEIS2 as robustly expressed in prostate, but not seminal vesicle, epithelial cells (9). Differential mRNA expression of *MEIS1* and *MEIS2* within the Swedish Watchful Waiting cohort was sufficient to discern an 18-month versus 40-month survival difference in patients with Gleason 6 and 7 tumors, respectively (9). These data suggested that retention of MEIS expression conferred a more favorable patient prognosis, indicating a tumor-suppressive role for MEIS expression in prostate cancer (9). More recently, Jeong and colleagues reported that MEIS2 expression was decreased in castration-resistant prostate cancer (CRPC) cells, and implicated MEIS2 as part of an intrinsic constitutively activated feed-forward signaling circuit formed during the emergence of CRPC (12). While these data implicate MEIS proteins as important in both prostate cancer initiation and progression to castration-resistant metastatic disease, studies to date have yet to define: (i) the prognostic utility of MEIS protein expression in progression to metastatic prostate cancer after radical prostatectomy; (ii) whether decreased expression of *both* MEIS1 and MEIS2 occurs in prostate tumors; and (iii) the functional necessity of MEIS expression to suppress tumor growth.

Here, we report that both *MEIS1* and *MEIS2* exhibit a step-wise decrease in expression during progression of prostate cancer from normal prostatic tissue, to localized prostate tumors, and finally to metastatic disease. We determine that *MEIS1* and *MEIS2* expression are significantly correlated in clinical datasets, demonstrating that expression of both *MEIS* genes is suppressed during prostate cancer progression. Using annotated tissue microarrays (TMA), we demonstrate that retention of MEIS expression is significantly associated with a lack of biochemical recurrence and clinically metastatic prostate cancer. We additionally show that MEIS-associated progression to metastatic prostate cancer is independent of known prognostic criteria, including Gleason grade. Analyses of RNA-sequencing (RNA-Seq) data from localized tumor and metastatic prostate cancer–identified genes associated with both loss of *MEIS* and metastatic prostate cancer progression, thereby elucidating potentially novel cancer progression pathways associated with *MEIS* loss. Pathways associated with MEIS expression in the primary tumor include targets of cMYC, proliferation, differentiation, and cell adhesion. In addition, we demonstrate that loss of MEIS expression in prostate cancer cells increases tumor growth *in vivo*. Together, these data support a significant functional role for MEIS proteins in prostate cancer, identify novel pathways associated with MEIS expression, and support the potential clinical utility of MEIS protein expression as a predictive biomarker of metastatic progression after radical prostatectomy.

Materials and Methods

Cell lines and materials

R1881 was purchased from Sigma-Aldrich and was stored at −20°C in ethanol. Human prostate cancer cell lines were grown as described previously (13, 14). All cultures were routinely screened for the absence of mycoplasma contamination using the ATCC Universal Mycoplasma Detection Kit. Dr. John Issacs at The Johns Hopkins University generously provided the LAPC-4 cell line, which has been previously characterized and cultured in Iscove's modified Eagle medium, 10% FCS, penicillin-streptomycin, and 1 nmol/L R1881 (13). Cell authentication of LAPC-4 cells was confirmed via DDC Medical services. RNA knockdown of *MEIS1* and *MEIS2* expression, both individual and dual knockdowns, was achieved using the pGIPZ lentiviral shRNA system (Dharmacon). Lines were experimentally analyzed within 10 passages of lentiviral gene delivery. Briefly, HEK293T packaging cells were plated in duplicate at $6E^6$ in 10-cm dishes. pGIPZ shRNA *MEIS1* and *MEIS2* plasmids were separately transfected using envelope and packaging vectors (Addgene) according to the manufacturer's instructions. Media containing the lentivirus were collected using a 0.45-μm filter and viral aliquots were added to 8.0-mL complete media and used to infect target LAPC-4 cells with 5 μg/mL polybrene for 24 hours. Complete media were then replaced followed by selection with puromycin (1 μg/mL, Invitrogen). Confirmation of knockdown of *MEIS1* and *MEIS2* was confirmed using both qRT-PCR and Western blotting.

Western blotting

Whole-cell lysates of 1×10^5 or more cells were used per lane. Western blotting was performed as reported previously (15). Briefly, cells were rinsed with cold PBS and scraped into RIPA buffer supplemented with protease inhibitors, sonicated twice, and resuspended in 4× sample buffer (Bio-Rad) supplemented with 10% β-mercaptoethanol (Sigma-Aldrich). The Pierce BCA Protein Assay Kit (Thermo Fisher Scientific) was used to determine protein concentration. Sixty micrograms of protein was loaded on a 10% SDS-polyacrylamide gel, electrophoresed, and transferred

to nitrocellulose membrane (LI-COR, Odyssey) overnight at 4°C. The membrane was blocked overnight in 5% nonfat milk in TBS at 4°C. Primary antibodies used were anti-MEIS1 (Ab19867, Abcam), anti-MEIS2 (ARP34683_P050, Aviva Systems Biology), anti-β-actin, (Clone AC-15, Sigma-Aldrich). The secondary antibodies goat anti-mouse IRDye 800 CW or donkey anti-rabbit IRDye 680 from LI-COR Biosciences were used, and images captured using an infrared Odyssey scanner (LI-COR).

qRT-PCR analyses

RNA was purified using the Qiagen RNeasy Mini Kit with the optional DNAse Digestion Kit (QIAGEN) and quality tested using an Agilent Bioanalyzer 2100 (Agilent Technologies). For standard qRT-PCR, extracted RNA was converted to cDNA by reverse transcription using SuperScript III Reverse Transcriptase (Invitrogen). Expression levels of *MEIS1*, *MEIS2*, and *RPL13A* transcript were quantified using Power SYBR Green Master Mix (Invitrogen) using custom primers that captured all isoforms for *MEIS1* and *MEIS2* (primer sequences in Supplementary Table S1). Expression levels of *MEIS*-associated targets were quantified using Power SYBR Green Master Mix (Invitrogen) using custom primers capturing the following genes: *AXIN2*, *cMYC*, *CD142 (F3)*, *FN1*, *ROCK1*, *SERPINE2*, *SNAI2*, and *TGF-β2*, (Supplementary Table S1). Standard curves were used to assess primer efficiency and average change in threshold cycle (ΔC_t) values was determined for each of the samples relative to endogenous RPL13A levels and compared with vehicle control ($\Delta\Delta C_t$). Experiments were performed in triplicate to determine mean SE, and Student *t* tests performed with normalization to control to obtain *P* values.

In vivo tumor formation

All animal studies were carried out in strict accordance with the recommendations in the Guide for the Care and Use of Laboratory Animals of the National Institutes of Health (Bethesda, MD). The protocol was approved by the University of Chicago Institutional Animal Care and Use Committee (IACUC, protocol number 72231). Ketamine/xylazine anesthesia was used for all surgical procedures, and all efforts were made to minimize suffering. *In vivo* tumor formation of derived lines of LAPC-4 was performed via a subcutaneous inoculation of 7.5×10^4 cells in 4- to 6-week-old male athymic nude mice (Harlan) using a 75% Matrigel (Corning) and 25% HBSS solution (BD Biosciences). Host mice were surgically castrated at least one week prior to cell inoculation and implanted with a subcutaneous 1.4-cm testosterone pellet to measure tumor take in a uniform androgen environment (16). Mice were allowed to recover and testosterone levels to equilibrate for 7 days before tumor injections.

Bioinformatics analysis of GEO arrays and RNA-Seq data

Microarray dataset. For human clinical cases, *MEIS1* and *MEIS2* expression was queried from publicly available Gene Expression Omnibus (GEO) datasets (GDS) of studies comparing benign prostate epithelia, benign prostate epithelia adjacent to prostate cancer, primary and metastatic tumors. We used one microarray dataset from the GEO database: GDS2545 containing 171 samples. Correlation in *MEIS1 and MEIS2* expression was determined using Pearson correlation coefficient, while Wilcoxon rank-sum tests and Kruskall–Wallis tests by ranks were used to determine differences in *MEIS1* and *MEIS2* expression between the above groups.

RNA-Seq dataset. We obtained raw RNA-Seq FASTQ files of 25 prostate tumors, 3 benign glands, and 51 annotated metastases via dbGAP (phs000310.v1.p1 for tumors and benign glands; phs000915.v1.p1 for metastases; refs. 17, 18). These datasets were chosen based upon the quality of mRNA, sequencing depth, and annotation. The tumor datasets are from patients who had undergone prostate surgery without prior therapy, and the metastases are from patients with castration-resistant prostate cancer, some of which had received taxane, enzalutamide, or abiraterone treatment (17, 18). The quality of raw reads was accessed by FastQC (v0.11.4). All reads were mapped to the human genome assembly (NCBI build 19) using STAR (v2.5.1b). Alignment metrics were collected by Picard tools (v2.8.1) and RSeQC (v2.6.4; ref. 19). Transcripts were assembled from the aligned reads using Cufflinks and combined with known gene annotation. The expression level of transcripts was quantified using FPKM (Fragments Per Kilobase of transcript per Million mapped reads)-based and read count–based methods. Transcript expression was normalized across samples. Primary tumor (PT) samples with *MEIS1* and *MEIS2* expression levels on the first tertile were classified as "Low MEIS Expression" group. Samples that belong to this group are SRR341197, SRR341199, SRR341202, SRR341203, and SRR341204 (DBGap phs000310.v1.p1; ref. 17). Samples with *MEIS1* and *MEIS2* expression levels on the third tertile were classified as "High MEIS Expression" group. It includes SRR341196, SRR341201, SRR341213, and SRR341217 (DBGap phs000310.v1.p1; ref. 17). Samples with FPKM <1.0 across all three categories (MEIS-High, MEIS-Low, and metastasis) were not included in our analyses. Differentially expressed genes (DEG) and isoforms were detected using Cuffquant-Cuffnorm-Cuffdiff suite (FPKM-based method, v2.2.1; ref. 20) and featureCounts (21), DESeq2 (v1.14.1; ref. 22), edgeR (v3.16.5; ref. 23), or limma (v3.30.8; ref. 24; read count-based method). Transcripts were further filtered by fold change ≥ 1.5. Genes detected by at least more than one method were collected to create a list of high-confidence DEGs. Biological insights from candidate gene lists were gained by performing gene-set enrichment analysis (GSEA) and Ingenuity Pathways Analysis (IPA; Ingenuity Systems) to identify functional categories or pathways that were significantly different.

GSEA leading edge analysis

Three leading edge analysis categories were user-defined *a priori* as gene sets involved in the cancer-related categories of "Cell Cycle & Proliferation"; "Adhesion & Motility"; and "Development, Differentiation, & Morphogenesis." Patient RNA-Seq data defined in Fig. 1 was loaded and run in GSEA 3.0 from the Broad institute (http://software.broadinstitute.org/gsea) to look for enrichment of gene sets in $MEIS^{High}$ tumors compared with $MEIS^{Low}$ tumors. Gene set groups from MSigDB that were included in initial GSEA analysis were GO (biological processes), Hallmark, Reactome, and KEGG. Once analysis was complete, enriched gene sets were ordered smallest to largest by FDR q-value for significance. Leading edge analysis categories were then populated with any gene set in which the title fit that category of interest and the FDR q-value was <0.1. Reactome pathways were excluded to prevent confounding results due to nearly identical gene sets being used under two different Reactome titles (Jacquard > 0.5). A leading edge analysis was then performed on each category separately using GSEA 3.0 to identify genes driving the enrichment of each category. For genes with at least 2 occurrences in an individual

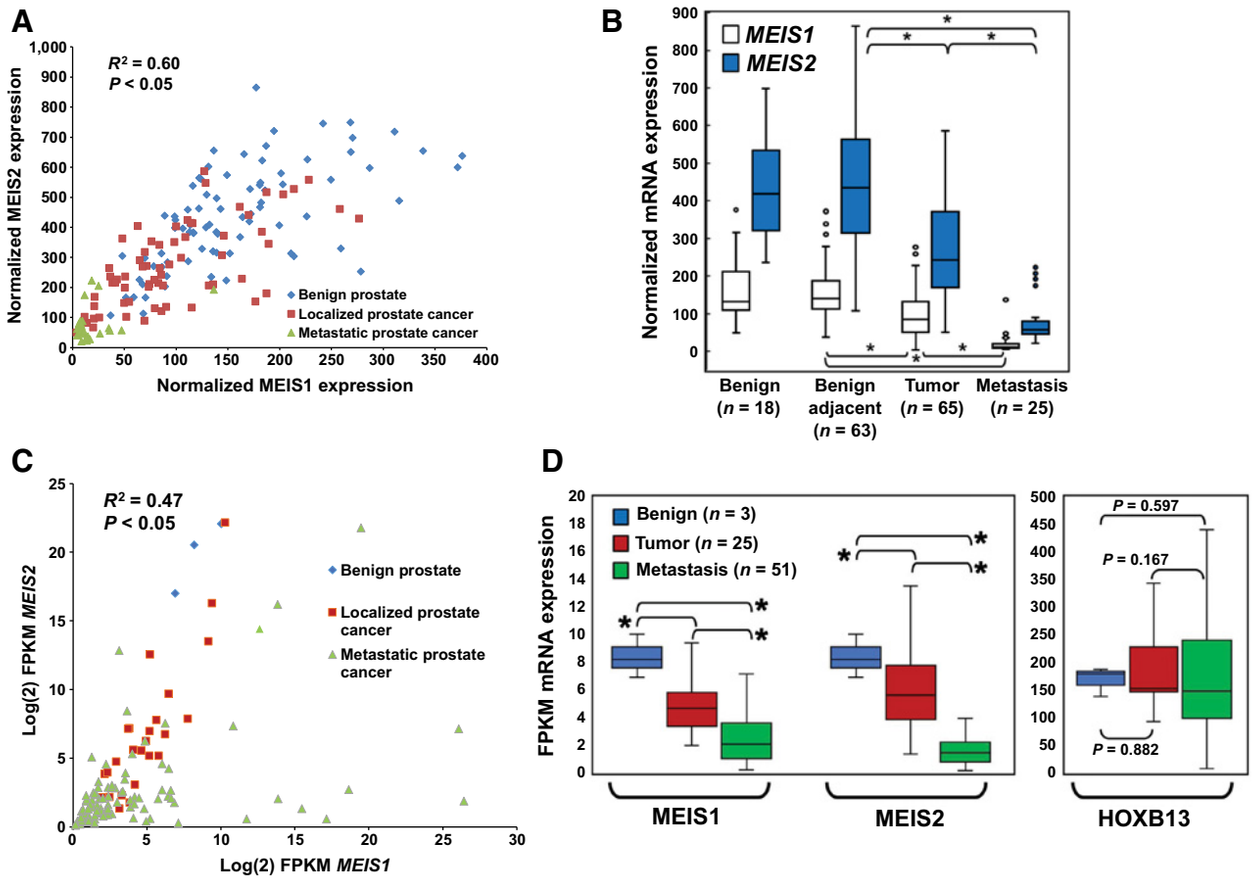

Figure 1.

Correlation of MEIS1 and MEIS2 expression and changes through prostate cancer progression. **A,** Scatter plot comparing *MEIS1* expression versus *MEIS2* expression from gene expression array data obtained from GDS2545. Benign prostate epithelia are in blue, localized prostate tumor are red, and metastatic prostate cancer are green. These data document coincident decreased expression of both MEIS1 and MEIS2 within prostate tumors and metastasis. **B,** Box and whisker plots of normalized mRNA expression of *MEIS1* (white) and *MEIS2* (blue) across benign prostate epithelia, benign prostate epithelia adjacent to tumor, localized prostate cancer, and metastatic prostate cancer (*$P < 0.05$). Gene array data obtained from GDS2545. **C,** Scatter plot comparing Log(2) FPKM expression between *MEIS1* (*x*-axis) and *MEIS2* (*y*-axis) using publicly available RNA-Seq tumor and metastasis datasets. Benign prostate epithelia are in blue, localized prostate tumor are red, and metastatic prostate cancer are green. These data again document a coincident decreased expression of both MEIS1 and MEIS2 within prostate tumors and metastasis. **D,** Box and whisker plots of log(2) FPKM of both *MEIS1, MEIS2, and HOXB13* in RNA-Seq datasets. Changes in mRNA expression of MEIS1, MEIS2, and HOXB13 between benign prostate epithelia (blue), localized prostate tumors (red), and prostate cancer metastases (green; *, $P < 0.05$). These data document significant step-wise decreases in MEIS1 and MEIS2 expression from benign to tumor to metastasis; no significant differences in HOXB13 expression were observed between benign epithelium, tumor, and metastasis.

category, the overlap between categories was determined using the intersect() command in R software (v3.4.0) to identify the most likely MEIS-associated genes with roles in prostate cancer progression and metastasis. A heatmap of log(2) FPKM values of the 47 overlapping genes from all three categories was then generated using the MORPHEUS online tool from Broad Institute (http://software.broadinstitute.org/morpheus/). Gene Ontology (GO) analysis was run on the 47 candidate genes, and results were limited to only those titles that had $P_{adj} < 0.05$ and referenced a clear and specific pathway, rather than a broader category or process.

Human tissue procurement and generation of tissue microarray for IHC

Two TMAs were procured for analysis of MEIS expression in prostate cancer. The University of Chicago Medical Center (UCMC) TMA was constructed by the Human Tissue Research Center at the UCMC with Institutional Review Board approval and has been described previously (25). TMA samples were not used for any nucleotide-based analyses, but only for IHC. Briefly, the TMA contains 138 treatment-naïve prostate cancer samples from radical prostatectomies performed at the University of Chicago between 1995 and 2002. Areas involved by prostate cancer and adjacent nonneoplastic prostatic tissue were punched (2-mm cores) from the formalin-fixed, paraffin-embedded samples and arrayed with 72–108 cores per slide. Preoperative characteristics including age, race, PSA, clinical tumor, node, metastasis (TNM) stage, and pathologic extension was collected. The second TMA was obtained from the Prostate Cancer Biorepository Network (PCBN). The PCBN TMA was constructed from 235 patients undergoing radical prostatectomy from 1982 to 2002 who were part of the "Natural History of Progression After PSA Elevation Following Radical Prostatectomy" study (26). The TMA

contains four cores each of normal and cancerous tissue per patient. Preoperative characteristics include age, race, BMI, PSA, primary, and secondary Gleason grades, and clinical stage. Postoperative characteristics include pathologic Gleason grades, and pathologic state (organ-confinement, extraprostatic extension, seminal vesicle involvement, or lymph node invasion). Of the 138 potential cases in the UCMC TMA, 39 cases were excluded because of lack of tissue on the slide or no prostate cancer was identified in the core. Of the 235 potential cases for analysis on the PCBN TMAs, 13 cases were excluded because no prostate cancer was identified on the core or tissue was missing from the slide. For both UCMC and PCBN TMAs, follow-up and outcome data were obtained. Postoperative outcomes of interest included surgical margin status, adjuvant or salvage external radiotherapy (XRT), and androgen deprivation therapy (ADT). Survival outcomes of interest included biochemical recurrence (BCR), defined as first detectable PSA after radical prostatectomy, and time to clinical metastasis, defined as radiographic or pathologic evidence of distant metastatic disease.

IHC staining and evaluation

IHC staining for MEIS (sc-81986 from Santa Cruz Biotechnology) was performed on formalin-fixed paraffin-embedded (FFPE) sections managed by the University of Chicago Human Tissue Resource Core facility. It should be noted that the sc-81986 antibody recognizes epitopes present on both MEIS1 and MEIS2 proteins, as demonstrated in Supplementary Fig. S1A–S1D. After deparaffinization and rehydration, tissues were treated with antigen retrieval buffer (S1699 from DAKO) in a steamer for 20 minutes. Anti-MEIS antibody at 1:300 was applied for 16 hours at 4°C in a humidity chamber. Following TBS wash, the antigen–antibody binding was detected with Envision+system (DAKO, K4001 for mouse primary antibodies) and DAB+Chromogen (DAKO, K3468). Tissue sections were briefly immersed in hematoxylin for counterstaining and were coverslipped.

Tissues were analyzed by a trained genitourinary pathologist and scored on percentage of cells with positive nuclear staining (0 = no staining; 1 = 1%–5% positive cells; 2 = 5%–50% positive cells; and 3 = 50%–100% positive cells). Patients were then divided into two groups for analysis: Patients with a composite score of 0–1 were considered MEIS negative, whereas patients with a score $\geq$2 were considered MEIS positive. For images, slides were digitized using a Pannoramic Scan Whole Slide Scanner (Cambridge Research and Instrumentation) and images captured using the Pannoramic Viewer software version 1.14.50 (3DHistech).

Statistical analysis

Statistical analyses were performed using Stata, version 13.0. Wilcoxon-rank sum, Kruskall–Wallis test by ranks, one-way ANOVA, Fisher exact tests, and χ^2 tests were used to compare baseline pre- and postoperative characteristics between MEIS-positive and MEIS-negative patients. Univariate analysis to determine whether MEIS score predicted time to BCR, and clinical metastasis, was conducted using Cox proportional hazard regression analysis, as well as Kaplan–Meier curves with log-rank tests. A multivariable Cox proportional hazard regression model was constructed to evaluate whether MEIS score predicted BCR and clinical metastasis.

For bioinformatics analysis, a Pearson correlation coefficient was used to determine linear correlation between *MEIS1* and *MEIS2* expression in both GEO and RNA-Seq datasets. Kruskall–Wallis test by ranks and Wilcoxon-rank sum tests was used to compare *MEIS1* and *MEIS2* expression between benign prostate epithelia, normal prostate epithelia adjacent to prostate cancer, localized prostate cancer, and metastatic prostate cancer in both datasets.

Results

Expression analyses reveal correlated expression of *MEIS1* and *MEIS2* and progressive loss of total *MEIS* expression during prostate cancer progression

To better understand the landscape of *MEIS1* and *MEIS2* expression, both in relation to each other and in relation to progression from benign to metastatic disease, expression analyses was conducted on two distinct publicly available gene expression datasets. The first dataset was the GEO GDS2545 microarray dataset derived from 170 prostate patient specimens; 10% of which were normal prostate epithelia ($n = 17$), 37% were benign prostate epithelia adjacent to prostate cancer ($n = 63$), 38% were localized prostate cancer ($n = 65$), and 15% were distant metastases ($n = 25$; ref. 27). The second dataset was comprised of two RNA-Seq datasets consisting of 79 patients, 4% of which were normal prostate epithelia ($n = 3$), 31% were localized prostate cancer ($n = 25$), and 65% were of metastatic prostate cancer ($n = 51$; refs. 17, 28).

We initially sought to determine whether one or both *MEIS* genes demonstrated correlative changes in expression among patient-derived datasets. Comparison of *MEIS1* to *MEIS2* expression in gene array datasets showed a significant positive correlation between *MEIS1* and *MEIS2* expression across benign, localized, and metastatic prostate cancer (Fig. 1A; $R^2 = 0.60$; $P < 0.05$). After determining that *MEIS1* and *MEIS2* expression are indeed positively correlated, we sought to identify the pattern of *MEIS1* and *MEIS2* expression changes across different biological states of the prostate, from benign prostate, localized prostate cancer, and metastatic prostate cancer. Comparative analyses demonstrate significant step-wise decreases in both *MEIS1* and *MEIS2* expression across normal prostate, localized prostate cancer and metastatic prostate cancer in the GEO dataset (Fig. 1B). Median *MEIS1* expression was nearly equivalent between benign prostate epithelia samples and normal prostate epithelia adjacent to tumor (131.2 vs. 140.3, $P > 0.05$). However, median *MEIS1* expression was significantly lower between normal prostate epithelia and localized prostate cancer (140.3 vs. 84.4, $P < 0.05$), and significantly lower still between localized and metastatic prostate cancer (84.4 vs. 11.1 $P < 0.05$). *MEIS2* expression followed a similar stepwise decrease, with median normalized expression decreasing from 434.7 in normal prostate epithelia adjacent to tumor, to 242.0 in localized, and 57.6 in metastatic prostate cancer (Fig. 1B, $P < 0.05$).

Similarly, comparison of *MEIS1* and *MEIS2* expression in an independent RNA-Seq dataset confirmed a significant positive correlation between *MEIS1* and *MEIS2* expression (Fig. 1C; $R^2 = 0.47$; $P < 0.05$; refs. 17, 28). Analyses of mRNA transcript quantitation likewise demonstrated a significant stepwise decrease in both MEIS1 and MEIS2 from benign epithelium to tumor (MEIS1: 8.37 to 4.95; MEIS2: 19.87 to 6.83; $P < 0.05$), and from tumor to metastasis (MEIS1: 4.95–3.52; MEIS2: 6.83–2.56; $P < 0.05$; Fig. 1D). Interestingly, there was no significant difference in HOXB13 mRNA expression different between benign, tumor, and metastatic tissues (benign: 167.68 FPKM, tumor: 197.39 FPKM,

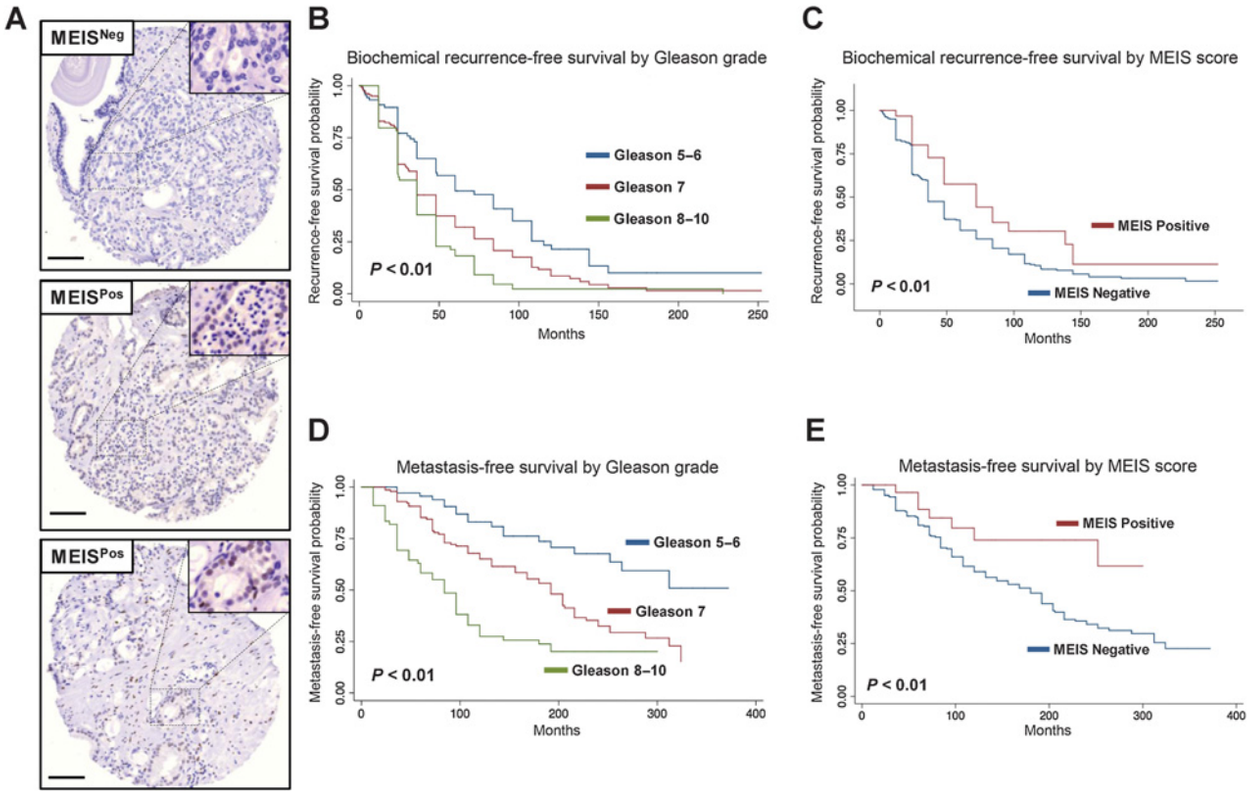

Figure 2.

IHC staining of prostate tissue and MEIS-associated BCR and metastasis. **A,** Representative staining of prostate tissue showing heterogeneity of total MEIS expression (10× magnification). Tumors with greater than 5% of cancer cells positive were considered MEIS-positive. **B–E,** Kaplan–Meier log-rank survival estimates of PSA-free survival for all patients stratified by Gleason grade low (5–6), intermediate (7), and high (8–10; **B**). **C,** Stratified by MEIS-negative tumors versus MEIS-positive tumors. Kaplan–Meier log-rank survival estimates of metastasis-free survival for all patients stratified by Gleason grade low (5–6), intermediate (7), and high (8–10; **D**). **E,** Stratified by MEIS-negative tumors versus MEIS-positive tumors.

metastases: 168.34 FPKM, $P = 0.356$; Fig. 1D). These data imply that, while mutations in HOXB13 are clearly important in prostate tumor imitation, changes in HOXB13 mRNA expression do not appear to be associated with cancer progression. However, the range of tumor MEIS expression does suggest the presence of a subset of tumors with high MEIS expression (Fig. 1C and D). Collectively, these data imply an important role for MEIS proteins in prostate cancer progression, and support a model whereby low *MEIS* tumor expression correlates with metastatic progression, or conversely that high *MEIS* tumor expression is associated with a lack of metastatic progression.

Tumor MEIS expression is associated with a lack of BCR and progression to clinically metastatic disease

Given the positive correlation of *MEIS1* and *MEIS2* expression and the identification of a decrease in both *MEIS1* and *MEIS2* through prostate cancer progression, we developed a robust and reliable IHC detection of both MEIS1 and MEIS2 to simultaneously detect both forms (Supplementary Fig. S1A–S1D). Furthermore, we validated a correlation between MEIS mRNA and protein expression by analyzing a series of primary prostate epithelial and stromal cultures (Supplementary Fig. S1E and S1F). We stained two different sets of prostate tissue microarrays, both of which included extensive patient annotation and follow-up. An *a priori* decision was made to identify tumors as "MEIS-positive" if their respective tissue samples contained greater than 5% of prostate cancer cells positive for MEIS expression (Fig. 2A). A total of 321 cases were stained for MEIS expression, with 11% ($n = 36$) positive for MEIS expression. Analyses of preoperative and perioperative characteristics documented that there was no difference in age, race, preoperative PSA, Gleason grade, clinical T stage, pathologic extension, or surgical margin status between the MEIS-positive and MEIS-negative tumors (Supplementary Table S2).

To determine whether MEIS expression was associated with prostate cancer progression, we analyzed postoperative outcomes between patients bearing either MEIS-positive or MEIS-negative tumors (Table 1). These analyses demonstrated that MEIS-negative patients are significantly more likely to have biochemical recurrence (84% vs. 56% $P < 0.01$) and clinically metastatic disease (51% vs. 19%, $P < 0.01$) compared with MEIS-positive patients. It is not surprising, then, that MEIS-negative patients are more likely to receive androgen deprivation therapy for metastatic disease compared with MEIS-positive patients (36% vs. 14%, $P = 0.02$). Similarly, MEIS-negative patients were nearly significantly more likely to receive some form of external radiotherapy (either for salvage therapy or metastatic disease) compared with MEIS-positive patients (29.2% vs. 25%, $P = 0.078$). However, despite

Table 1. Postoperative outcomes between MEIS-positive and MEIS-negative tumors

	<5% Cell MEIS Positive (%)	>5% Cell MEIS Positive (%)	*P*
BCR, *n* (%)			<0.001
No	46 (16.1)	16 (44.4)	
Yes	239 (83.9)	20 (55.6)	
ADT, *n* (%)			0.02
None/unknown	135 (47.4)	24 (66.7)	
Salvage	47 (16.5)	7 (19.4)	
For metastatic disease	103 (36.1)	5 (13.9)	
XRT, *n* (%)			0.078
None/unknown	202 (70.9)	27 (75)	
Salvage	80 (28.1)	7 (19.4)	
For metastatic disease	3 (1.1)	2 (5.6)	
Metastasis, *n* (%)			<0.001
No metastasis	137 (48.9)	29 (80.6)	
Clinical metastasis	143 (51.1)	7 (19.4)	
Cancer-specific survival, *n* (%)			0.036
Alive	179 (62.8)	29 (80.6)	
Dead from PCa	106 (37.2)	7 (19.4)	
Overall survival, *n* (%)			0.075
Alive	126 (44.2)	22 (61.1)	
Dead	159 (55.8)	14 (38.9)	

a higher proportion of patients receiving additional treatment for prostate cancer progression in the MEIS-negative group, there was a higher proportion of cancer-specific death in the MEIS-negative group compared with the MEIS-positive group (37% vs. 19%, $P = 0.036$).

In our cohort, time to BCR was determined as months between radical prostatectomy and first positive postoperative PSA. Of the 321 patients available for survival analysis, one patient was excluded due to lack of follow-up. Post-radical prostatectomy BCR occurred in 81% ($n = 259$) patients. The median recurrence-free survival (RFS) time was 36 months for the entire cohort. Figure 2B shows BCR of all patients stratified by Gleason grade into low (GG 5–6), intermediate (GG 7), and high (GG 8–10) risk groups. As expected, patients with higher Gleason grade had worse RFS compared with the lower Gleason grade group (log-rank, $P < 0.01$). Figure 2C shows BCR stratified by MEIS score. Median follow-up time was 36 months in MEIS-negative and 48 months in MEIS-positive tumor-bearing patients. A positive MEIS score was significantly associated with improved BCR-free survival compared with a negative MEIS score, with 5- and 10-year recurrence-free survival of 57% and 30% in MEIS positive patients, compared with 5- and 10-year recurrence-free survival of 31% and 9% in MEIS-negative patients, respectively (log-rank, $P < 0.01$). Using a univariate Cox analysis, a positive MEIS score is associated with a lower risk of BCR (HR = 0.57). These data support that a positive MEIS score in primary prostate tumors is associated with lower risk of BCR, and that tumor MEIS expression may exhibit a more indolent clinical course of prostate cancer progression.

While biochemical recurrence is frequently utilized as a surrogate marker to assess prostate cancer progression, it is known that not all patients with BCR will progress to clinically metastatic disease (2). Therefore, we analyzed our TMA datasets to determine whether positive MEIS expression was associated with a lack of progression to clinically metastatic disease, defined as radiographic or pathologic evidence of distant cancer metastasis. Of the 321 patients available for analysis, 8 patients were excluded for lack of follow-up. Progression to clinically metastatic disease occurred in 47% ($n = 150$) of patients in our cohort. The median metastasis-free survival (MFS) time was 96 months for the entire cohort. Figure 2D shows MFS of all patients stratified by Gleason grade into low (GG 5–6), intermediate (GG 7), and high (GG 8–10) risk groups. Similar to the BCR data in Fig. 2B, patients with higher Gleason grade had worse MFS compared with the lower Gleason grade group (log-rank, $P < 0.01$). Figure 2E illustrates MFS stratified by MEIS score. Median follow up time was 96 months in MEIS-negative patients and 91 months in MEIS-positive patients. A positive MEIS score was significantly associated with improved MFS compared with a negative MEIS score, with a 10-year MFS of 74% in MEIS-positive patients, compared with only 59% in MEIS-negative patients, respectively (log rank, $P = 0.0133$). A univariate Cox analysis demonstrated that a positive MEIS score is associated with a lower risk of progression to clinically metastatic disease (HR = 0.40). Given the critical importance and treatment ramifications in identifying patients likely to progress to true clinically metastatic prostate cancer, we performed a multivariate Cox regression analysis to determine whether positive MEIS score was predictive of a lower risk of clinically metastatic disease independent of known prognostic factors (Table 2). Adjusting for age, race, preoperative PSA, clinical T stage, Gleason grade, pathologic extension, and surgical margin status, a positive MEIS score was still predictive of a lower risk of clinically metastatic disease compared with MEIS-negative patients (Table 2; multivariate HR = 0.28, $P = 0.033$). Taken together, these data demonstrate that a positive MEIS score in primary prostate tumors is independently associated with a lower risk of progression to metastatic disease, implying that MEIS proteins play a significant clinical role in stratifying patients at risk for prostate cancer progression.

Identification of *MEIS*-associated networks and gene sets involved in prostate cancer progression

Given that protein expression of MEIS1 and MEIS2 expression was significantly associated with a lack of biochemical recurrence and progression to clinically metastatic disease, we hypothesized that comparing $MEIS^{High}$ to $MEIS^{Low}$ tumors would identify differentially expressed gene sets and networks associated with prostate cancer progression. Moreover, differentially expressed genes between $MEIS^{High}$ to $MEIS^{Low}$ tumors would identify genes associated with MEIS expression and function. Using the RNA-seq datasets described in Fig. 1, we stratified our primary prostate tumors into tertiles, and compared differentially expressed genes (DEG) between $MEIS^{High}$ vs. $MEIS^{Low}$ tumors, as well as all metastatic specimens to identify potential *MEIS*-associated genes involved in prostate cancer progression (Fig. 3A). As expected, based upon our subgrouping, both *MEIS1* and *MEIS2* expression were significantly greater in the $MEIS^{High}$ group compared with either the $MEIS^{Low}$ tumor group as well as the metastatic group (Fig. 3A). Furthermore, *MEIS* expression is not significantly different between the $MEIS^{Low}$ tumors and metastatic prostate cancer (Fig. 3A). Pairwise analyses identified 1,804 DEG between the $MEIS^{High}$ and $MEIS^{Low}$ prostate primary tumor groups which also demonstrated similar and nonsignificant expression between the $MEIS^{low}$ and metastatic samples (Fig. 3B; Supplementary Table S3). These genes thus have similar expression between more aggressive $MEIS^{Low}$ tumors and metastasis, yet significantly distinct expression in the more indolent $MEIS^{High}$ tumors. These DEGs were analyzed using both Ingenuity Pathway Analysis (IPA) and Gene Ontology (GO) to identify candidate gene sets and

Table 2. Multivariate analyses of MEIS-positive versus MEIS-negative tumors

	Risk of BCR		Risk of clinical metastasis	
	HR (95% CI)	***P***	**HR (95% CI)**	***P***
MEIS Percent				
<5%	Ref	Ref	Ref	Ref
>5%	0.76 (0.43–1.37)	0.37	0.28 (0.08–0.90)	0.03
Age	1.02 (0.99–1.05)	0.18	0.98 (0.95–1.02)	0.39
Race				
White	Ref	Ref	Ref	Ref
Other	0.68 (0.25 –1.81)	0.44	0.29 (0.07–1.27)	0.10
PSA	1.00 (0.99–1.02)	0.66	0.99 (0.97–1.01)	0.43
Gleason grade				
5–6	Ref	Ref	Ref	Ref
3+4 or 4+3	1.28 (0.76–2.17)	0.35	1.51 (0.66–3.46)	0.33
8–10	1.57 (0.89–2.74)	0.12	2.58 (1.09–6.12)	0.03
Clinical T stage				
T1	Ref	Ref	Ref	Ref
T2	1.17 (0.70–1.95)	0.56	2.42 (0.96–6.09)	0.06
T3–4	1.08 (0.50–2.34)	0.85	2.95 (0.94–9.22)	0.06
Pathologic extension				
Organ confined	Ref	Ref	Ref	Ref
Extra-prostatic extension	1.21 (0.62–2.39)	0.58	0.99 (0.37–2.70)	0.99
Seminal vesicle invasion	1.45 (0.65–3.25)	0.37	2.20 (0.76–6.38)	0.15
Lymph node positive	1.84 (0.87–3.90)	0.11	2.62 (0.95–7.20)	0.06
Surgical margins				
T1	Ref	Ref	Ref	Ref
T2	1.18 (0.81–1.71)	0.40	0.75 (0.45–1.25)	0.26

networks associated with both *MEIS* expression and prostate cancer progression (Fig. 3C and D). IPA identified several networks involved in cellular proliferation and survival, as well as inflammatory response and cellular movement (Fig. 3C). Gene Ontology (GO) analyses identified pathways that are significantly associated with smooth muscle contraction, vasoconstriction, microtubule anchoring, cell-to-cell adhesion, and regulation of cell junction assembly (Fig. 3D). Further analyses utilizing gene set enrichment analyses (GSEA), which incorporates directionality of gene changes between groups, documented that more indolent $MEIS^{High}$ tumors have decreased expression of MYC targets and genes involved in G_1–S transition, and increased expression of genes involved in cell fate commitment, cell–cell adhesion, negative regulation of proliferation, and cell morphogenesis and differentiation (Fig. 3E). Indeed, previous data from Zebrafish have demonstrated regulation of Myc by Meis proteins (29). Collectively, these analyses support a model whereby MEIS-positive prostate tumors are less proliferative, more differentiated, and have increased cell–cell adhesion, thereby promoting a more indolent tumor phenotype.

Loss of both MEIS1 and MEIS2 is associated with increased tumor growth *in vivo*

Given our clinical and bioinformatic data support the hypothesis that tumor *MEIS* expression confers a more favorable clinical prognosis, we hypothesized that depletion of *MEIS* expression in prostate cancer cells would result in a more aggressive tumor phenotype. To begin elucidating how MEIS expression is decreased in prostate tumors, we analyzed TCGA datasets for promoter methylation, as well as utilized pharmacologic approaches to increase MEIS expression in cell lines. These data demonstrated significant promoter methylation of MEIS1, and our ability to increase MEIS2 expression utilizing three distinct HDAC inhibitors (Supplementary Fig. S2). To test the phenotypic and function impact of depleting MEIS expression, we created LAPC-4 prostate cancer cells harboring knockdowns of *MEIS1*, *MEIS2*, and both *MEIS1* and *MEIS2* (Fig. 4). Figure 4A illustrates knockdown of both MEIS1 and MEIS2 mRNA and protein. *In vivo* subcutaneous xenografts of LAPC-4 cells depleted of both MEIS1 and MEIS2 demonstrate a significant increase in tumor size within 25 days postinjection, with an 185 mm^3 and 159 mm^3 increase in mean tumor volume compared with controls at day 27 and 29, respectively (Fig. 4B; $P < 0.05$). Interestingly, single knockdown of either *MEIS1* or *MEIS2* demonstrates that decreased expression of either individual MEIS protein alone is not sufficient to enable increased tumor volume, as there was no difference in mean tumor volume between either *MEIS1* or *MEIS2* knockdown and controls (Supplementary Fig. S3A). These data support a role for MEIS proteins in negatively regulating tumor growth, as their depletion led to increased tumor volume over time *in vivo*.

Based upon our analyses of clinical RNA-Seq specimens, we sought to identify and validate the expression of several key genes associated with differences in tumor MEIS expression. Initial GSEA analyses of patient-derived RNA-Seq specimens determined that prostate tumors with higher MEIS expression appear to be less proliferative, more differentiated, and have increased cell–cell adhesion, thus encouraging a less aggressive tumor phenotype (Fig. 3). In an attempt to identify specific molecular targets associated with MEIS expression in prostate cancer, we used those three phenotypic categories to develop a GSEA leading edge analysis. This analysis first identified genes driving the enrichment of gene sets involved in cell cycle and proliferation; development, differentiation, and morphogenesis; or adhesion and motility (Fig. 4C; Supplementary Fig. S3B). The intersection of leading edge genes occurring in all three phenotypic categories identified 47 candidates associated with MEIS expression in prostate cancer (Fig. 4C; Supplementary Fig. S3B).

To validate the association between MEIS expression and the expression of candidate factors that have established roles in

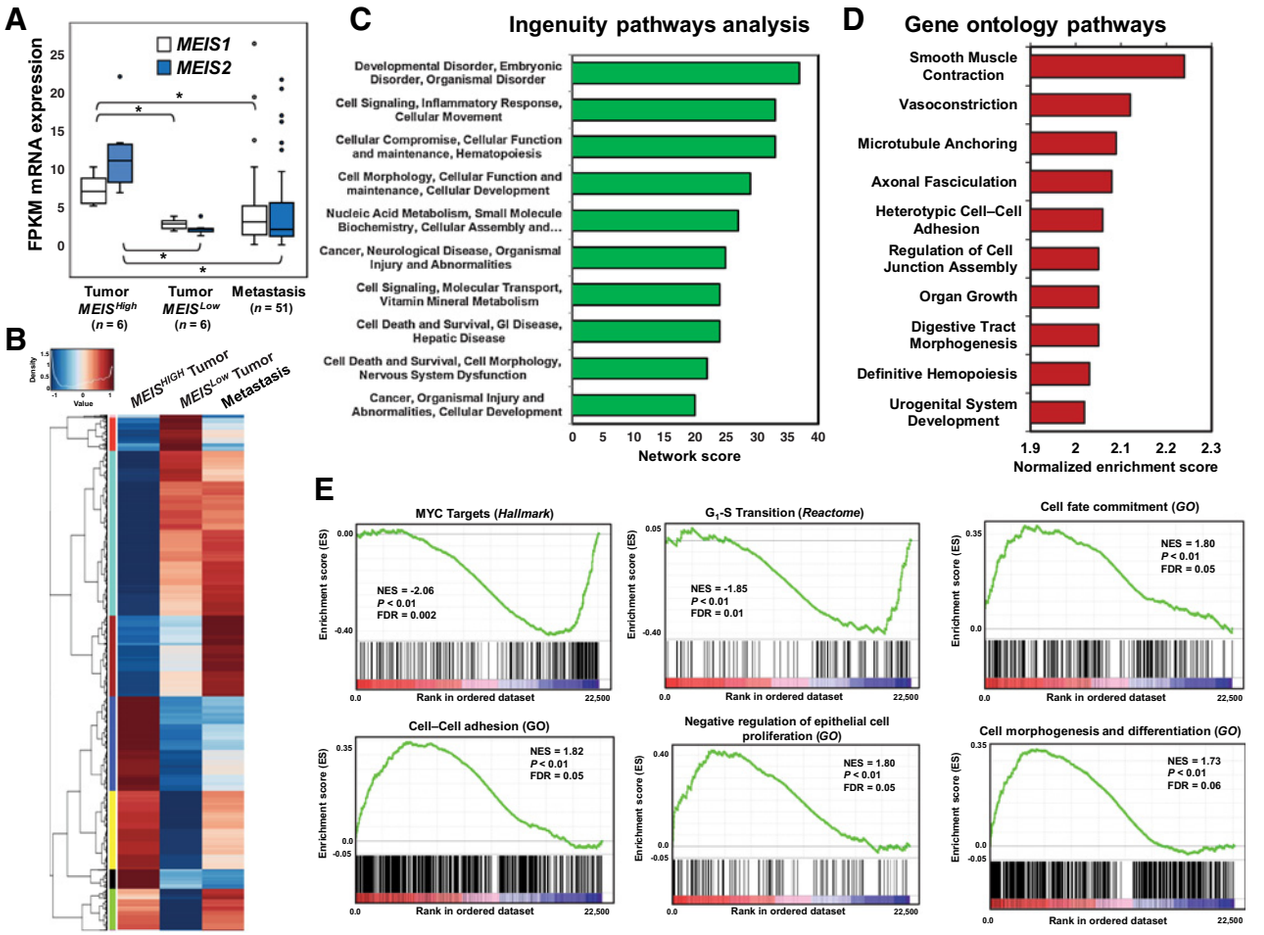

Figure 3.

Identification of gene sets and networks associated with MEIS and prostate cancer progression. **A,** Box and whisker plots of *MEIS1* and *MEIS2* mRNA expression in $MEIS^{High}$ tumors ($n = 6$), $MEIS^{Low}$ tumors ($n = 6$), and metastases ($n = 51$) from RNA-Seq datasets. FPKM values for all genes were used to identify genes that were similar between $MEIS^{Low}$ tumors and metastasis, and significantly different (1.5-fold, FDR < 0.05) in the $MEIS^{High}$ tumors. **B,** Heatmap of differentially expressed genes between $MEIS^{High}$ (left), $MEIS^{Low}$ (center), and metastatic prostate cancer (right). Scores range from low expression (blue) to high expression (red). Gene lists and FPKM values are listed in Supplementary Table S3. **C,** Ingenuity Pathway Analysis (IPA) of the top ten networks derived from differentially expressed gene set between $MEIS^{High}$, $MEIS^{Low}$, and metastatic prostate cancer datasets. **D,** Top ten Gene Ontology (GO) Biological Processes derived arranged by normalized enrichment score of differentially expressed gene set between $MEIS^{High}$, $MEIS^{Low}$, and metastatic prostate cancer datasets. **E,** GSEA of significantly altered pathways between $MEIS^{High}$ and $MEIS^{Low}$ tumors. Normalized enrichment scores (NES) demonstrate that $MEIS^{High}$ tumors have decreased expression of cMYC targets and genes regulating G_1–S transition, and increased expression of genes involved in in cell fate commitment, cell–cell adhesion, negative regulators of cell proliferation, and cell morphogenesis and differentiation. Gene sets were obtained and analyzed against the Hallmark, Gene Ontology (GO), and Reactome datasets.

prostate cancer progression, we conducted qRT-PCR on a series of candidate genes identified by our GSEA analyses, leading edge analyses, and genes with established roles in tumor progression using our LAPC-4 MEIS-knockdown cells. The fold change in mRNA expression within the MEIS-depleted cells was then compared with the fold change expression between $MEIS^{High}$ versus $MEIS^{Low}$ tumors (Fig. 4D). Importantly, we observed significantly increased expression of cMYC mRNA in LAPC-4 cells that had depleted MEIS expression. Deviant expression of the cell surface glycoprotein CD142 (also known as coagulation factor 3, or F3), the serine protease SerpinE2 (Serpin Family E Member 2), and the matrix protein FN1 (Fibronectin 1) have been implicated in several cancers for its tumor-promoting effects as well as their roles in remodeling the tumor microenvironment (30–32). In LAPC-4 cells with depleted MEIS expression, we observe a significant increase in CD142 expression, and decreased expression of SERPINE3 and FN1 (Fig. 4D). In all instances, the directional change in expression matches that of $MEIS^{Low}$ versus $MEIS^{High}$ tumors, whereby when MEIS is depleted in LACP-4 cells, the change in expression correlates similarly with $MEIS^{Low}$ tumor expression (Fig. 4D). Changes in these genes upon MEIS knockdown suggest that changes in local tumor environment may play a role in MEIS-associated increases in tumor volume *in vivo*.

Decreased expression of AXIN2 is associated with cellular invasion and proliferation as well poor prognosis in prostate cancer and regulation of cMYC pathway members (33, 34). Changes in the expression of TGFβ2 (Transforming growth factor beta 2) are also implicated in prostate cancer progression (35, 36).

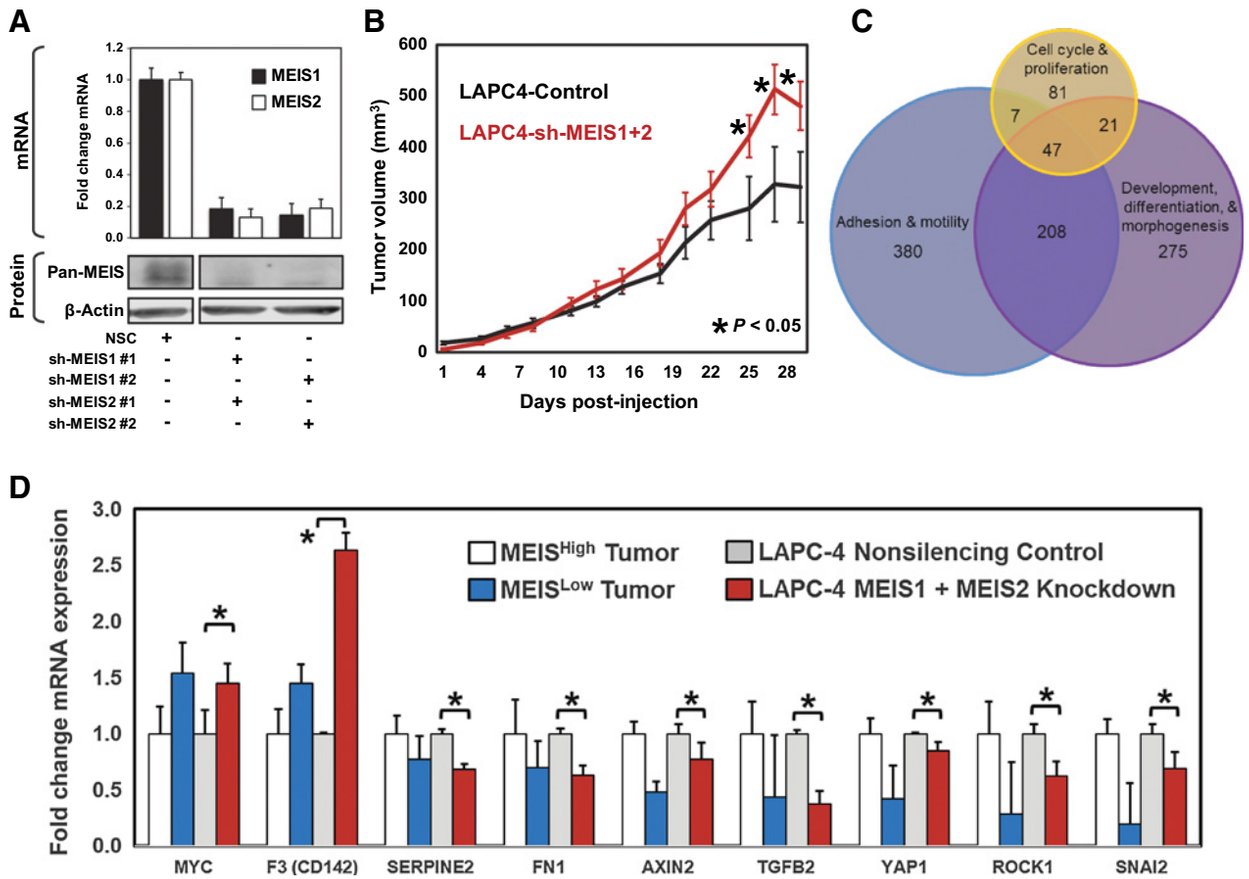

Figure 4.

Functional characterization of total MEIS knockdown LAPC-4 cells. **A,** Assessment of MEIS1 and MEIS2 knockdown in LAPC-4 cell using RT-PCR (top) and Western blot analysis (bottom). Two shRNA constructs against *MEIS1* and two shRNA constructs against *MEIS2* were utilized to control for off-target effects. To determine MEIS1 and MEIS2 protein levels after shRNA depletion, Western blot analyses was conducted using a mouse monoclonal targeting both MEIS1 and MEIS2 (Pan-MEIS). **B,** Xenograft growth of MEIS1 and MEIS2 double knockdown LAPC-4 cells injected subcutaneously on the flanks of hormonally intact male nude mice compared with nonsilencing controls. Differences in tumor volumes at days 25, 27, and 29 postinjection were statistically significant (Control $N = 8$; double knockdown $N = 8$; * $P < 0.05$). **C,** Venn diagram of MEIS-associated genes prioritized using GSEA leading edge analyses. The GSEA leading edge analyses identifies genes that potentially drive a phenotype, and are consistently at the "leading edge" of multiple pathway categories. This analysis was performed on pathways associated with Cell Cycle and Proliferation, Adhesion and Motility, and Development, Differentiation and Morphogenesis, and leading edge genes common to all three were identified ($n = 47$). A heatmap demonstrating differential expression of these 47 genes is shown in Supplementary Fig. S3B. **D,** Quantitative real-time PCR mRNA analyses of candidates using cDNA of MEIS1 and MEIS2 double knockdown LAPC-4 cells compared with nonsilencing controls. Data represents mean and SEM of experiments conducted in triplicate (*, $P < 0.05$). The fold change in mRNA expression within LAPC-4 cells with MEIS depletion is graphed next to the fold change in expression between $MEIS^{High}$ vs. $MEIS^{Low}$ tumors, which was statistically tested using RNA-seq analyses platforms to identify DEGs.

ROCK1 (Rho Associated Coiled-Coil Containing Protein Kinase 1) is a protein serine/threonine kinase that is activated when bound to the GTP-bound form of RHO; expression and genetic variation of ROCK1 has an established role in prostate cancer progression and has been reported to function via cMYC (37, 38). SNAI2 (Snail Family Transcriptional Repressor 2, also referred to as SLUG) is a member of the Snail family of C2H2-type zinc finger transcription factors and is critically involved in regulating epithelial–mesenchymal transitions (EMT). Downregulation of SNAI2 is associated with increased EMT and regulation of E-cadherin (39–41). In both prostate tumor RNA-Seq datasets, and via qRT-PCR in LAPC-4 cells with depleted MEIS1 and MEIS2, we observe decreased expression of AXIN2, TFGβ2, ROCK1, and SNAI2 (Fig. 4D, $P < 0.05$ for LAPC-4 analyses). Collectively, these data implicate a causal function for MEIS1 and MEIS2 expression in regulating genes involved in cancer progression and metastasis, including cMYC, cMYC targets, and critical mediators of cell adhesion and differentiation.

Discussion

Here we demonstrate that expression of MEIS1 and MEIS2 have a significant role in blocking prostate cancer progression and metastasis. We observe a stepwise decrease in the expression of both genes from benign prostate epithelia to localized prostate cancer and further still with progression to metastatic prostate cancer. Furthermore, we have shown that subsequent retention of total MEIS expression in localized prostate cancer is

significantly associated with a lack of BCR and progression to clinically metastatic disease. Finally, we have demonstrated that loss of both MEIS proteins is necessary to increase tumor growth *in vivo*, and that this phenotype is associated with changes in pathways that regulate cell proliferation, cell adhesion and motility, and cellular differentiation and morphogenesis. Together, these data support the hypothesis that retention of MEIS expression in prostate cancer confers a more indolent prostate cancer phenotype, with a decreased propensity for metastatic progression.

Germline mutations of HOXB13, particularly the G84E mutation, have been identified in men with early-onset familial prostate cancer and validated in several cohorts (6, 42). Furthermore, recent evidence suggests that the G84E mutation confers a more aggressive phenotype of prostate cancer, with G84E patients having a significantly higher diagnosis PSA, higher Gleason score, and a higher likelihood of positive surgical margins at time of radical prostatectomy (43). Based upon data presented here, one potential mechanism of HOXB13(G84E)-associated tumor aggressiveness could result from a disruption or modulation of MEIS interaction by the G84E mutation, leading to defective MEIS–HOX signaling and a loss of MEIS-mediated tumor suppression. We document that HOXB13 mRNA expression is not significantly different between normal prostate epithelia, prostate tumors, and metastasis; this observation implies that expression changes in HOX cofactors such as MEIS1 and MEIS2, but perhaps not HOX proteins themselves, have a more significant role in prostate cancer progression.

While our study suggests that retention of MEIS proteins leads to a clinically more indolent form of prostate cancer using a combination of bioinformatic, histologic, and *in vivo* approaches, it is not without limitations. First, while our bioinformatics data strongly suggest a step-wise loss of both MEIS proteins through prostate cancer across multiple datasets, we lack the granularity necessary to observe changes in MEIS through cancer progression within individual patients or through our model systems. Second, while our TMA datasets included a relatively large sample size of patients, only 11% of patients were positive for MEIS expression, and so our results would likely need to be subsequently validated using larger datasets. Finally, while our data strongly supports previous studies that implicate MEIS as prognostic in prostate cancer, and that loss of MEIS results in increased tumor growth, we have yet to identify the exact mechanism by which loss of MEIS confers a more aggressive prostate cancer phenotype. One potential mechanism, purported by Cui and colleagues, suggests that MEIS1 negatively regulates AR function, and thus retention of tumor MEIS expression could confer a more active and prodifferentiation function for AR (44, 45). However, our data does suggest a number of candidate MEIS-associated genes that regulate cell proliferation and the local tumor microenvironment. Ultimately, these limitations also present obvious future directions for research, which include mouse models that develop metastatic prostate cancer, analyses of metastatic prostate cancer samples from patients, and ChIP-Seq–based approaches to mechanistically decipher MEIS function.

Clinically, the identification of HOX cofactors such as MEIS serves two primary purposes. First, the ability to develop new biomarkers to better risk stratify patients is greatly needed. Indeed, in this study, we demonstrate that MEIS expression can be prognostic for BCR and metastasis in the postprostatectomy setting, which has implications for the length and aggressiveness of surveillance patterns and for the use of adjuvant or salvage therapies. Several large randomized trials have shown that use of adjuvant radiotherapy is associated with greater BCR-free survival compared with observation for patients undergoing radical prostatectomy with high-risk features, but this was at the cost of increased short and long-term side effects (46, 47). Given that MEIS expression was associated with a lower hazard of biochemical recurrence and clinical metastasis independent of known prognostic risk factors, utilizing biomarkers such as MEIS may enable better risk stratification of patients leading to appropriate aggressive response for those at highest risk of disease progression, while avoiding harmful side effects in those with more indolent disease. Second, while survival for prostate cancer has continued to improve, it remains the second leading cause of cancer-related death among American men. As such, there need to be continued efforts to identify novel gene networks and pathways that confer more aggressive prostate cancer behavior, as these genes may represent potentially novel targets for future therapies. Our data suggests that MEIS proteins may represent a previously largely unexplored target for the identification of efficacious targets and the development of future cancer therapeutics.

Disclosure of Potential Conflicts of Interest

No potential conflicts of interest were disclosed.

Authors' Contributions

Conception and design: R.R. Bhanvadia, H. Brechka, D.J.V. Griend
Development of methodology: R.R. Bhanvadia, C. VanOpstall, H. Brechka, M. Gillard
Acquisition of data (provided animals, acquired and managed patients, provided facilities, etc.): R.R. Bhanvadia, C. VanOpstall, H. Brechka, N.S. Barashi, M. Gillard, E.M. McAuley, J.M. Vasquez, G. Paner, A.M. Demarzo, M. Han
Analysis and interpretation of data (e.g., statistical analysis, biostatistics, computational analysis): R.R. Bhanvadia, C. VanOpstall, M. Gillard, W.-C. Chan, J. Andrade, R.Z. Szmulewitz, D.J.V. Griend
Writing, review, and/or revision of the manuscript: R.R. Bhanvadia, C. VanOpstall, H. Brechka, N.S. Barashi, M. Gillard, E.M. McAuley, G. Paner, W.-C. Chan, J. Andrade, M. Han, R.Z. Szmulewitz, D.J.V. Griend
Administrative, technical, or material support (i.e., reporting or organizing data, constructing databases): N.S. Barashi, E.M. McAuley
Study supervision: D.J.V. Griend

Acknowledgments

We wish to acknowledge the support of the University of Chicago Section of Urology led by Dr. Arieh Shalhav, the Department of Surgery led by Dr. Jeff Matthews, and the Ben May Institute for Cancer Research led by Dr. Geoffrey Greene. We would also like to acknowledge the support of the University of Chicago Comprehensive Cancer Center (UCCCC) led by Dr. Michelle Le Beau. We would also like to thank Dr. William Isaacs from the Johns Hopkins Brady Urologic Institute for his mentorship, encouragement, and guidance on the project. We also with to thank expert technical assistance of the Human Tissue Resource Center core facility led by Dr. Mark Lingen, and the assistance of Mary Jo Fekete. We also thank the Immunohistochemistry Core Facility run by Terri Li. We also thank the Center for Research Informatics analysis group led by Dr. Jorge Andrade. This work was supported by grants DODPCRPPC130587 (principal investigator: D.J.V. Griend); NWU/UC/NSUHS Prostate SPORE (P50 CA180995; principal investigator: Catalona); the University of Chicago Comprehensive

Cancer Center (UCCCC), especially the Cancer Center Support Grant (P30CA014599). H. Brechka and C. VanOpstall were supported by the Cancer Biology Training Grant (T32 CA009594). E.M. McAuley is supported by an F31 from the NIDDK (DK111131). R.R. Bhanvadia is supported by a University of Chicago Pritzker School of Medicine Fellowship and National Institute of Diabetes and Digestive and Kidney Diseases (NIDDK) grant #2T35DK062719-27. J.M. Vasquez is funded by The University of Chicago PREP Program (NIH R25GM066522). The Center for Research Informatics is funded by the Biological Sciences Division at the University of Chicago with additional funding provided by the Institute for Translational Medicine NIH CTSA grant number UL1 TR000430. This work was also supported by the Department of Defense Prostate cancer Research Program, DOD award no. W81XWH-10-2-0056 and W81XWH-10-2-0046 PCRP Prostate cancer Biorepository Network (PCBN) and the NIH/NCI prostate SPORE pathology core (award no. 5P50CA058236).

The costs of publication of this article were defrayed in part by the payment of page charges. This article must therefore be hereby marked *advertisement* in accordance with 18 U.S.C. Section 1734 solely to indicate this fact.

Received December 8, 2017; revised March 23, 2018; accepted April 26, 2018; published first May 1, 2018.

References

1. Siegel RL, Miller KD, Jemal A. Cancer statistics, 2017. CA Cancer J Clin 2017;67:7–30.
2. Paller CJ, Antonarakis ES. Management of biochemically recurrent prostate cancer after local therapy: evolving standards of care and new directions. Clin Adv Hematol Oncol 2013;11:14–23.
3. Eifler JB, Feng Z, Lin BM, Partin MT, Humphreys EB, Han M, et al. An updated prostate cancer staging nomogram (Partin tables) based on cases from 2006 to 2011. BJU Int 2013;111:22–9.
4. Brechka H, Bhanvadia RR, VanOpstall C, Vander Griend DJ. HOXB13 mutations and binding partners in prostate development and cancer: function, clinical significance, and future directions. Genes Dis 2017;4: 75–87.
5. Longobardi E, Penkov D, Mateos D, De Florian G, Torres M, Blasi F. Biochemistry of the tale transcription factors PREP, MEIS, and PBX in vertebrates. Dev Dyn 2014;243:59–75.
6. Ewing CM, Ray AM, Lange EM, Zuhlke KA, Robbins CM, Tembe WD, et al. Germline mutations in HOXB13 and prostate-cancer risk. N Engl J Med 2012;366:141–9.
7. Li W, Huang K, Guo H, Cui G. Meis1 regulates proliferation of non-small-cell lung cancer cells. J Thorac Dis 2014;6:850–5.
8. Crijns AP, de Graeff P, Geerts D, Ten Hoor KA, Hollema H, van der Sluis T, et al. MEIS and PBX homeobox proteins in ovarian cancer. Eur J Cancer 2007;43:2495–505.
9. Chen JL, Li J, Kiriluk KJ, Rosen AM, Paner GP, Antic T, et al. Deregulation of a Hox protein regulatory network spanning prostate cancer initiation and progression. Clin Cancer Res 2012;18:4291–302.
10. De Marzo AM, Platz EA, Sutcliffe S, Xu J, Gronberg H, Drake CG, et al. Inflammation in prostate carcinogenesis. Nat Rev Cancer 2007;7:256–69.
11. Curry PT, Atherton RW. Seminal vesicles: development, secretory products, and fertility. Arch Androl 1990;25:107–13.
12. Jeong JH, Park SJ, Dickinson SI, Luo JL. A constitutive intrinsic inflammatory signaling circuit composed of miR-196b, Meis2, PPP3CC, and p65 drives prostate cancer castration resistance. Mol Cell 2017;65: 154–67.
13. Litvinov IV, Vander Griend DJ, Xu Y, Antony L, Dalrymple SL, Isaacs JT. Low-calcium serum-free defined medium selects for growth of normal prostatic epithelial stem cells. Cancer Res 2006;66:8598–607.
14. D'Antonio JM, Vander Griend DJ, Antony L, Ndikuyeze G, Dalrymple SL, Koochekpour S, et al. Loss of androgen receptor-dependent growth suppression by prostate cancer cells can occur independently from acquiring oncogenic addiction to androgen receptor signaling. PLoS One 2010;5: e11475.
15. Kregel S, Kiriluk KJ, Rosen AM, Cai Y, Reyes EE, Otto KB, et al. Sox2 is an androgen receptor-repressed gene that promotes castration-resistant prostate cancer. PLoS One 2013;8:e53701.
16. Sedelaar JP, Dalrymple SS, Isaacs JT. Of mice and men-warning: Intact versus castrated adult male mice as xenograft hosts are equivalent to hypogonadal versus abiraterone treated aging human males, respectively. Prostate 2013;73:1316–25.
17. Pflueger D, Terry S, Sboner A, Habegger L, Esgueva R, Lin PC, et al. Discovery of non-ETS gene fusions in human prostate cancer using next-generation RNA sequencing. Genome Res 2011;21:56–67.
18. Robinson D, Van Allen EM, Wu YM, Schultz N, Lonigro RJ, Mosquera JM, et al. Integrative clinical genomics of advanced prostate cancer. Cell 2015;161:1215–28.
19. Wang L, Wang S, Li W. RSeQC: quality control of RNA-seq experiments. Bioinformatics 2012;28:2184–5.
20. Trapnell C, Williams BA, Pertea G, Mortazavi A, Kwan G, van Baren MJ, et al. Transcript assembly and quantification by RNA-Seq reveals unannotated transcripts and isoform switching during cell differentiation. Nat Biotechnol 2010;28:511–5.
21. Liao Y, Smyth GK, Shi W. featureCounts: an efficient general purpose program for assigning sequence reads to genomic features. Bioinformatics 2014;30:923–30.
22. Love MI, Huber W, Anders S. Moderated estimation of fold change and dispersion for RNA-seq data with DESeq2. Genome Biol 2014;15:550.
23. Robinson MD, McCarthy DJ, Smyth GK. edgeR: a Bioconductor package for differential expression analysis of digital gene expression data. Bioinformatics 2010;26:139–40.
24. Ritchie ME, Phipson B, Wu D, Hu Y, Law CW, Shi W, et al. limma powers differential expression analyses for RNA-sequencing and microarray studies. Nucleic Acids Res 2015;43:e47.
25. Szmulewitz RZ, Chung E, Al-Ahmadie H, Daniel S, Kocherginsky M, Razmaria A, et al. Serum/glucocorticoid-regulated kinase 1 expression in primary human prostate cancers. Prostate 2012;72:157–64.
26. Pound CR, Partin AW, Eisenberger MA, Chan DW, Pearson JD, Walsh PC. Natural history of progression after PSA elevation following radical prostatectomy. JAMA 1999;281:1591–7.
27. Chandran UR, Ma C, Dhir R, Bisceglia M, Lyons-Weiler M, Liang W, et al. Gene expression profiles of prostate cancer reveal involvement of multiple molecular pathways in the metastatic process. BMC Cancer 2007;7:64.
28. Robinson D, Van Allen EM, Wu YM, Schultz N, Lonigro RJ, Mosquera JM, et al. Integrative clinical genomics of advanced prostate cancer. Cell 2015;162:454.
29. Bessa J, Tavares MJ, Santos J, Kikuta H, Laplante M, Becker TS, et al. meis1 regulates cyclin D1 and c-myc expression, and controls the proliferation of the multipotent cells in the early developing zebrafish eye. Development 2008;135:799–803.
30. Han X, Guo B, Li Y, Zhu B. Tissue factor in tumor microenvironment: a systematic review. J Hematol Oncol 2014;7:54.
31. Smirnova T, Bonapace L, MacDonald G, Kondo S, Wyckoff J, Ebersbach H, et al. Serpin E2 promotes breast cancer metastasis by remodeling the tumor matrix and polarizing tumor associated macrophages. Oncotarget 2016;7: 82289–304.
32. Ifon ET, Pang AL, Johnson W, Cashman K, Zimmerman S, Muralidhar S, et al. U94 alters FN1 and ANGPTL4 gene expression and inhibits tumorigenesis of prostate cancer cell line PC3. Cancer Cell Int 2005; 5:19.
33. Shojima K, Sato A, Hanaki H, Tsujimoto I, Nakamura M, Hattori K, et al. Wnt5a promotes cancer cell invasion and proliferation by receptor-mediated endocytosis-dependent and -independent mechanisms, respectively. Sci Rep 2015;5:8042.
34. Hu BR, Fairey AS, Madhav A, Yang D, Li M, Groshen S, et al. AXIN2 expression predicts prostate cancer recurrence and regulates invasion and tumor growth. Prostate 2016;76:597–608.
35. Lu T, Burdelya LG, Swiatkowski SM, Boiko AD, Howe PH, Stark GR, et al. Secreted transforming growth factor beta2 activates NF-kappaB, blocks apoptosis, and is essential for the survival of some tumor cells. Proc Natl Acad Sci U S A 2004;101:7112–7.

36. Zeng L, Kyprianou N. Apoptotic regulators in prostatic intraepithelial neoplasia (PIN): value in prostate cancer detection and prevention. Prostate Cancer Prostatic Dis 2005;8:7–13.
37. Liu K, Li X, Wang J, Wang Y, Dong H, Li J. Genetic variants in RhoA and ROCK1 genes are associated with the development, progression and prognosis of prostate cancer. Oncotarget 2017;8:19298–309.
38. Zhang C, Zhang S, Zhang Z, He J, Xu Y, Liu S. ROCK has a crucial role in regulating prostate tumor growth through interaction with c-Myc. Oncogene 2014;33:5582–91.
39. Esposito S, Russo MV, Airoldi I, Tupone MG, Sorrentino C, Barbarito G, et al. SNAI2/Slug gene is silenced in prostate cancer and regulates neuroendocrine differentiation, metastasis-suppressor and pluripotency gene expression. Oncotarget 2015;6:17121–34.
40. Xie Y, Liu S, Lu W, Yang Q, Williams KD, Binhazim AA, et al. Slug regulates E-cadherin repression via p19Arf in prostate tumorigenesis. Mol Oncol 2014;8:1355–64.
41. Little GH, Baniwal SK, Adisetiyo H, Groshen S, Chimge NO, Kim SY, et al. Differential effects of RUNX2 on the androgen receptor in prostate cancer: synergistic stimulation of a gene set exemplified by SNAI2 and subsequent invasiveness. Cancer Res 2014;74:2857–68.
42. Beebe-Dimmer JL, Hathcock M, Yee C, Okoth LA, Ewing CM, Isaacs WB, et al. The HOXB13 G84E mutation is associated with an increased risk for prostate cancer and other malignancies. Cancer Epidemiol Biomarkers Prev 2015;24:1366–72.
43. Storebjerg TM, Hoyer S, Kirkegaard P, Bro F, LuCamp Study G, Orntoft TF, et al. Prevalence of the HOXB13 G84E mutation in Danish men undergoing radical prostatectomy and its correlations with prostate cancer risk and aggressiveness. BJU Int 2016;118:646–53.
44. Cui L, Li M, Feng F, Yang Y, Hang X, Cui J, et al. MEIS1 functions as a potential AR negative regulator. Exp Cell Res 2014;328:58–68.
45. Vander Griend DJ, Litvinov IV, Isaacs JT. Conversion of androgen receptor signaling from a growth suppressor in normal prostate epithelial cells to an oncogene in prostate cancer cells involves a gain of function in c-Myc regulation. Int J Biol Sci 2014;10:627–42.
46. Thompson IM, Tangen CM, Paradelo J, Lucia MS, Miller G, Troyer D, et al. Adjuvant radiotherapy for pathological T3N0M0 prostate cancer significantly reduces risk of metastases and improves survival: long-term follow up of a randomized clinical trial. J Urol 2009;181:956–62.
47. Bolla M, van Poppel H, Tombal B, Vekemans K, Da Pozzo L, de Reijke TM, et al. Postoperative radiotherapy after radical prostatectomy for high-risk prostate cancer: long-term results of a randomised controlled trial (EORTC trial 22911). Lancet 2012;380:2018–27.
48. Guo Y, Sheng Q, Li J, Ye F, Samuels DC, Shyr Y. Large scale comparison of gene expression levels by microarrays and RNAseq using TCGA data. PLoS One 2013;8:e71462.
49. Price ME, Cotton AM, Lam LL, Farre P, Emberly E, Brown CJ, et al. Additional annotation enhances potential for biologically-relevant analysis of the Illumina Infinium HumanMethylation450 BeadChip array. Epigenetics Chromatin 2013;6:4.
50. Diez-Villanueva A, Mallona I, Peinado MA. Wanderer, an interactive viewer to explore DNA methylation and gene expression data in human cancer. Epigenetics Chromatin 2015;8:22.
51. Welsbie DS, Xu J, Chen Y, Borsu L, Scher HI, Rosen N, et al. Histone deacetylases are required for androgen receptor function in hormone-sensitive and castrate-resistant prostate cancer. Cancer Res 2009;69:958–66.